Article

High-Triplet-Energy Polymers via RAFT Polymerization: Synthesis and Properties

Heorhi K. Belavusau [1,2,⊥], Melika Ghasemi [3,⊥], Aliaksei A. Vaitusionak [1], Irina V. Vasilenko [1], Matvei V. Patsai [1,2], Dmytro Volyniuk [3], Juozas V. Grazulevicius[3,*], Sergei V. Kostjuk[4,*]

[1] Research Institute for Physical Chemical Problems of the Belarusian State University, 14 Leningradskaya St., 220006 Minsk, Belarus

[2] Department of Chemistry, Belarusian State University, 14 Leningradskaya st., 220006 Minsk, Belarus

[3] Department of Polymer Chemistry and Technology, Kaunas University of Technology, K. Barsausko str. 59, Kaunas 51423, Lithuania

[4] Sorbonne Universite, CNRS, Institut Parisien de Chimie Moleculaire, Equipe Chimie des Polymeres, 4 place Jussieu, 75252 Paris Cedex 05, France

***** Correspondence: sergei.kostjuk@sorbonne-universite.fr, juozas.grazulevicius@ktu.lt

Abstract: RAFT polymerization of a series of styrene-type dibenzoheterocyclic monomers bearing carbazole, phenoxazine, 9,9-dimethylacridane and phenothiazine moieties using S-dodecyl-S′-(α,α′-dimethyl-α″-acetic acid)trithiocarbonate as a chain transfer agent has been investigated. The corresponding polymers with the controlled molar mass of up to 30,000 g·mol^{-1} with low to moderate dispersity (Đ = 1.2-1.6) were synthesized. The thermal, photophysical and electrochemical properties of the prepared polymers have been investigated using their solutions, films and *in silico* to establish the structure-properties relationship. The synthesized polymers were characterized by high values of HOMO (up to -5 eV), singlet (up to 3.8 eV) and triplet (up to 3.2 eV) energies, which are responsible for their unique properties such as formation of excimers with $CHCl_3$ and dichloromethane or the ability to undergo coupling via electrooxidation in case of poly(9,9-dimethyl-10-(4-vinylphenyl)-9,10-dihydroacridan). Subsequently, two series of OLEDs based on the synthesized polymers were fabricated in order to study the charge-injecting and charge-transporting properties of these materials as well as to evaluate their performance in solution-processable diodes.

Keywords: RAFT polymerization, high triplet energy polymers, OLEDs, excimer emission

⊥ These authors contributed equally.

1. Introduction

Currently, high triplet energy materials are of great interest to researchers given the extensive utilization of their properties in the fabrication of organic light-emitting diodes (OLEDs) [1-4], photovoltaic [5-7] and photocatalytic processes [8-11]. Thus, in the development of new generations of OLEDs, whose operation is based on the principles of phosphorescence and thermally activated delayed fluorescence (TADF), an essential objective is the efficient harvesting of triplet excitons [12]. Accordingly, a specific requirement is imposed on the host material of the emission layer of OLEDs: its triplet energy must exceed that of the corresponding guest (emitter), which for blue diodes exceeds 2.8 eV [13]. In the context of solar cells, a significant process involved in the conversion of electromagnetic radiation is triplet–triplet annihilation (TTA), in which it is extremely important to be able to control the level of the triplet state in order to facilitate the utilization of photons with a certain energy [8,10]. As for photocatalytic systems, in the majority of them, the triplet excited state of catalyst is responsible for the activation of C-X bonds (X = Hal, H, etc.), which find a wide application in polymer [14,15] and organic chemistry [16,17]. Therefore, the accurate design of compounds with tuned triplet energy enables achieving high efficiency and selectivity of these processes.

In recent years, polymeric materials are increasingly being preferred, due to their capacity to facilitate OLEDs fabrication through more accessible solution-based methodologies [18-22]. This enhancement in accessibility is particularly noteworthy, as it enables the optimization of the morphological stability of the active layers that constitute the device architecture [13,21,22]. In addition, cross-linked high triplet energy polymers are promising as heterogenous photocatalysts and for sensing applications [23,24].

The classical design of high triplet energy polymers involves the modification of various donor compounds based on dibenzoheterocyclic moieties (carbazole [25-30], phenoxazine [15,27,31,32], acridan [27,33-37], phenothiazine [11,14,30], dibenzofuran [39,40], dibenzothiophene [27,40]) by incorporation of polymerizable group. Importantly, the step-growth polymerization methods that lead to an increase in the conjugation system of the donor fragment are not desired since above-mentioned conjugation results in a substantial decrease in HOMO and the triplet energies compared to those of the monomers [41,42]. This complicates the control of properties and limits the utilization of such materials. Consequently, chain-growth polymerization methods via radical [25,43,44], cationic [45], anionic [18] and ring-opening [29,46] mechanisms are frequently employed for preservation of energy characteristics of the original donor moieties.

Among the different techniques mentioned above, the radical polymerization appeared to be the most promising for the synthesis of such polymers due to the its applicability to the wide range of donor-based vinyl monomers. Indeed, the cationic polymerization of electron-reach styrene-based monomers is accompanied by competitive step-growth mechanism that hinders effective control over the polymer architecture [45]. For the present study RAFT technique was chosen as an approach to the polymerization processes, since it, being user-

friendly and not requiring the use of heavy metal compounds in contrast to classical ATRP, allows polymerizing in a controlled fashion a wide range of monomers [47,48].

In this work, we developed an approach for the preparation of polymers with high triplet energy which consists of varying different donor increments in dibenzoheterocyclic moieties of styrene-type monomers. For this purpose, well-defined polymer with M_n(SEC) ≤ 30,000 g·mol^{-1}, moderate dispersity (Đ = 1.2-1.6) and good thermal properties (T_g = 182-200 °C, T_{ID} = 333-404 °C) were synthesized via RAFT polymerization of styrene-type monomers with carbazole, phenoxazine, acridan and phenothiazine substituents. The study of electrochemical, photophysical properties in conjunction with DFT calculations allowed to establish the rational design of polymer structure to achieve high triplet energy. The distinctive properties of these polymers make them interesting to various fields including photocatalysis (especially, C-Hal photoactivation) and the synthesis of electro- and photo-sensitive materials. These polymers were also tested as hosts for solution-processable OLEDs, however further optimization is required to reach adequate external quantum efficiency.

2. Experimental

2.1. Materials

Cyclohexanone (Sigma-Aldrich, ≥ 99%) was dried overnight with CaH_2 and then distilled from CaH_2 under reduced pressure. THF (Sigma-Aldrich, ≥ 99%) was treated with KOH and distilled twice from Na under an inert atmosphere. Toluene (Sigma-Aldrich, ≥ 99%) was refluxed with Na and distilled twice from Na under an inert atmosphere. S-Dodecyl-S′-(α,α′-dimethyl-α″-acetic acid)trithiocarbonate (DDMAT) was synthesized according to the published procedure [49]. 2,2'-Azobisisobutyronitrile (AIBN) (Sigma-Aldrich, ≥ 98%) was recrystallized from ethanol. $CDCl_3$ (Euriso-top®), $CHCl_3$ (Sigma-Aldrich, 99.5%), methanol (Sigma-Aldrich, 99.9%) and ethanol (Sigma-Aldrich, 96%) were used as received.

2.2. Instrumentation

^{1}H (500 MHz) NMR spectra of the synthesized monomers were recorded in $CDCl_3$ at 25 °C on a Bruker Avance III spectrometer. Mass spectra were obtained by the electron impact mass spectrometry (EI-MS) on GSMS-QP2010 Plus. Size exclusion chromatography (SEC) was performed on an Ultimate 3000 Thermo Scientific apparatus with Agilent PLgel 5 μm MIXED-C (300×7.5 mm) column and one precolumn (PLgel 5 μm guard 50×7.5 mm) thermostated at 30 °C. The detection was achieved by differential refractometer (thermostated at 35 °C). Tetrahydrofuran (THF) was eluted at a flow rate of 1.0 ml min^{-1}. The calculation of molecular weights and polydispersity was carried out using polystyrene standards (Polymer Labs, Germany). Differential scanning calorimetry (DSC) and thermogravimetric analysis (TGA) measurements were carried out using a Netzsch STA (Simultaneous thermal analysis) 449 F3 device at a heating rate of 20 °C min^{-1} under nitrogen flow. UV–vis and photoluminescence spectra of dilute solutions were recorded with the

PerkinElmer Lambda 25 UV VIS spectrometer and Edinburgh Instruments FLS980 spectrometer, respectively. For these measurements, the dilute solutions of the investigated compounds were prepared by dissolving them in a spectral grade THF at 10^{-4} M concentration. Edinburgh Instruments FLS980 spectrometer (excitation wavelength of 300 nm) and PicoQuant LDH-DC-375 laser (wavelength 374 nm) as the excitation source were used for recording photoluminescence (PL) decay curves. Photoluminescence quantum yields (PLQY) of THF solutions were recorded using an integrated sphere (inner diameter of 120 mm). Cyclic voltammetry (CV) measurements were performed using a micro-Autolab III (Metrohm Autolab) potentiostat-galvanostat. A three-electrode cell equipped with a glassy carbon working electrode, an Ag/Ag^+ reference electrode and a glassy carbon counter electrode were employed. The measurements were performed for anhydrous dichloromethane with 0.1 M of tetrabutylammonium hexafluorophosphate (Bu_4NPF_6) as the supporting electrolyte under nitrogen atmosphere at a scan rate of 50 $mV \cdot s^{-1}$. The measurements were calibrated using ferrocene/ferrocenium (FC) system, as an internal standard. The solid-state ionisation potentials (IP_{PE}) were estimated by electron photoemission spectrometry in ambient air. The samples were spin-coated onto fluorine-doped tin oxide (FTO)-coated glass substrates, which were cleaned in acetone, izopropanol, were dried in argon, and were treated by UV-ozone for 30 minutes. A 30 W deep UV deuterium light source (180–400 nm) ASBN-D130-CM from Spectral Products©, coupled with a CM110 1/8 m monochromator, was employed to expose the samples to monochromatic light. The photocurrent generated under illumination was recorded using a Keithley 6517B electrometer, a high-resistance meter, connected to the counter electrode. The energy scan of the incident photons was performed by gradually increasing their energy. This was accomplished by adjusting wavelengths from 280 nm to 180 nm in 1 nm increments using the monochromator. Indium-tin-oxide (ITO)-coated substrates, with a sheet resistance of 5 Ω per square and pixels with an active area of 4.5 mm^2, were cleaned by Hellmanex solution, deionized water, isopropanol, followed by drying with argon, and treatment with UV-ozone for 30 minutes. The structure of the OLEDs is was ITO/HAT-CN (8nm)/VM-35 (40nm)/EML (20nm) /TSPO1 (8nm)/TPBi (40nm)/LiF (1.7)/AL (devices I) and ITO/HAT-CN (8nm)/VM-35 (40nm)/EML (Polymers and POT2T (50%)) (20nm)/TSPO1 (8nm)/TPBi (40nm)/LiF (1.7)/Al. For the fbrication of devices of the both series, VM-35 and the EML were spin-coated, while the rest of the layers were thermally evaporated under a vacuum of 2×10^{-6} mbar, using vacuum equipment from Kurt J. Lesker inside MB EcoVap4G glove box. For the preparation of the layer of VM-35, 12 mg of the compound was dissolved in 1.5 mL of chlorobenzene using sonification and filtered through a 0.2 μm syringe filter. For spin coating, 70 μl of the solution was deposited onto the substrate at 2000 rmp for 80 s inside the glovebox under inert atmosphere. The samples were pre-anneaed at 100 °C for 30 min, followed by annealing at 200 °C for 60 min. For the preparation of the EML of devices **I-P1–P4**, 4 mg of AcDbp and **P1–P4** were dissolved separatly in 1 mL of THF and then combined according to the required host-to-guest ratio. Then, 70 μL of the solution was depsited onto the substrate and spin-coated at 3500 rmp for 80s inside the glovebox under inert atmosphere. The samples were annealed at 80°C for 30 min and left to cool down. After spin-coating, the cathode was cleaned with acetone and by isopropanol. For the second series

of OLEDs (**I I-P1–P4**), the layers of VM-35 was prepared as it is described above. For the EML, the compounds were combined taking into account their molecular weight for exciplex formation. For PO-T2T, 4 mg and **P1**, **P2**, **P3**, and **P4**, 1.31 mg, 1.38 mg, 1.5 mg, and 1.45 mg of the compound swere dissolved in 1 mL of THF and combined at 50 wt%, in the molar ratio of 1:1. Then 100 µl of the solution were deposited onto the substrates and were spin-coated at 2000 rmp for 70 s inside the glovebox. The samples were annealed at 80 °C for 30 min.The similar cleaning procedure used for device I was applied for the fabrication of device **II**. A sourcemeter (Keithley 2400C) and certificated photodiode (PH100-Si-HA-D0), together with the energy monitor (11S-LINK), were used for the estimation of current density in reference to voltage and luminance in reference to voltage characteristics of the non-passivated fabricated devices under the ambient air. A calibrated photodiode was used to measure the brightness. UV-visible Avantes AvaSpec-2048XL spectrometer was employed to record the electroluminescent spectra.

2.3. Synthesis of monomers

The styrene-type monomers **M1**-**M4** were synthesized using modified method applied earlier in our previous works [51]. Briefly, 9*H*-carbazole (4.11 g, 24.6 mmol), (or 10*H*-phenoxazine (4.51 g, 24.6 mmol); or 9,9-dimethylacridan (5.15 g, 24.6 mmol), or 10*H*-phenothiazine (4.90 g, 24.6 mmol)), *bis*(di-*tert*-butyl(4-dimethylaminophenyl)phosphine)dichloropalladium(II) (Pd(amphos)Cl_2, 162 mg, 0.23 mmol), 4-bromostyrene (3 g, 16.38 mmol) and sodium *tert*-butoxide (3.20 g, 33.3 mmol) were dissolved under argon in 135 mL of dry toluene and stirred for 10 min at room temperature (preformation of the catalyst). The reaction mixture was heated at 90 °C for 8 h. After cooling, the reaction mixture was diluted with dichloromethane and the organic phase was washed with water and brine. After being dried over Na_2SO_4 and filtered, the solvent was removed, and the residue was purified by column chromatography using the mixture of hexane and dichloromethane in a volume ratio of 6:1 as eluent. The target products were recrystallized from hexane. NMR spectral and MS data for monomers **M1**–**M4** are presented in Supplimentary Materials (Experimental Section, Fig. S1).

2.4. Polymerization procedure

Polymerization was carried out under dry argon atmosphere in a Schlenk tube. Liquid reagents were transferred to reactor via dry syringes against a continuous argon flow. In a typical polymerization experiment, 115 µL of solution of DDMAT in cyclohexanone (30, 12 or 2.4 mM for $[M]_0/[I]_0$ = 40, 100 and 500, respectively) and 115 µL of solution of AIBN in cyclohexanone (10, 4, 0.8 mM for $[M]_0/[I]_0$ = 40, 100 and 500, respectively) were sequentially added to solid monomer (230 mmol). After three freeze-pump-thaw cycles the reaction was started by immersing Schlenk tube into an oil bath preheated to 70 ℃. After a predetermined time, a portion of solution was withdrawn and poured into excess of ethanol. The precipitated polymers were separated from the solution by centrifugation and then were dried in vacuum at 50 ℃. Before analyses, copolymers were reprecipitated twice from $CHCl_3$ into methanol. Monomer conversions were determined gravimetrically.

3. Results and Discussions

3.1. Synthesis of polymers P1-4

In the first step of the present research, a series of substituted styrene monomers was synthesized (**M1**–**M4**) in one stage via palladium catalyzed Buchwald–Hartwig condensation of 1-bromo-4-vinylbenzene with corresponding N-heterocyclic compound (Fig. 1a).

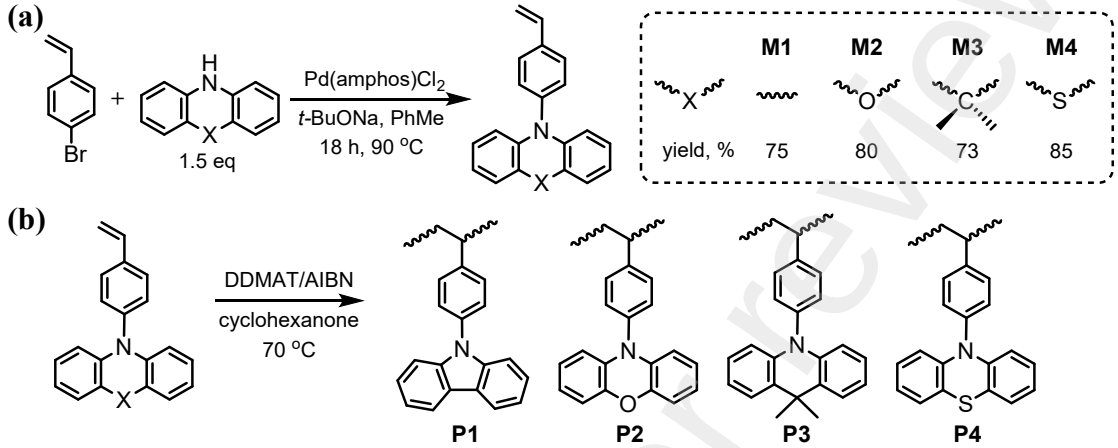

Figure 1. (a) The scheme of **M1-M4** synthesis; (b) their RAFT-mediated polymerization using S-dodecyl-S′-(α,α′-dimethyl-α′′-acetic acid)trithiocarbonate (DDMAT) as chain-transfer agent.

Styrene-type monomers were obtained with relatively high yields (73-85 %) and their structures were confirmed by ^{1}H NMR spectroscopy and MS. After a comparative analysis of the ^{1}H NMR spectra of four monomers (Fig. 2, Fig. S1), it seems possible to emphasize some common and specific features of them. Most of the protons of the styrene fragment (**a-c**) show a similar series of signals for all monomers: CH_2 protons (**a'** and **a**) produce two doublets with a large difference in shift value (5.36-5.38 ppm for **a'** and 5.83-5.87 ppm for **a**); methyne proton (**b**) is charachterized by doublet of doublets (6.79-6.84 ppm); aromatic protons (**c**) give doublet (6.62-6.67 ppm). Other aromatic protons of styrene moiety (**d**) show a similar doublet (7.30-7.34 ppm) only for monomers **M2**–**M4**, however, for **M1** this signal is shifted to the weaker field region (7.54 ppm). This phenomenon could be explained by the difference in dihedral angle (d_a) between N-heterocyclic moiety and styrene fragment: for **M1** $d_a = 55$ degrees, while for **M2**–**M4** $d_a = 90$ degrees (values were calculated using computational model describing below). It leads to rapprochement (and increased interaction) of **d** and **e** protons as well as the appearance of mesomeric effect of carbazole on the electron density of styrene in **M1**, causing a change in the chemical shift value. Each signal responsible for protons (**e**-**h**) of N-heterocyclic fragment show the same multiplicity at different values of the chemical shift for **M2**–**M4**, while series of signals for **M1** differ in both of multiplicity and in chemical shift, that is associated with the absence of increment X (Fig. 1) in the structure of carbazole moiety.

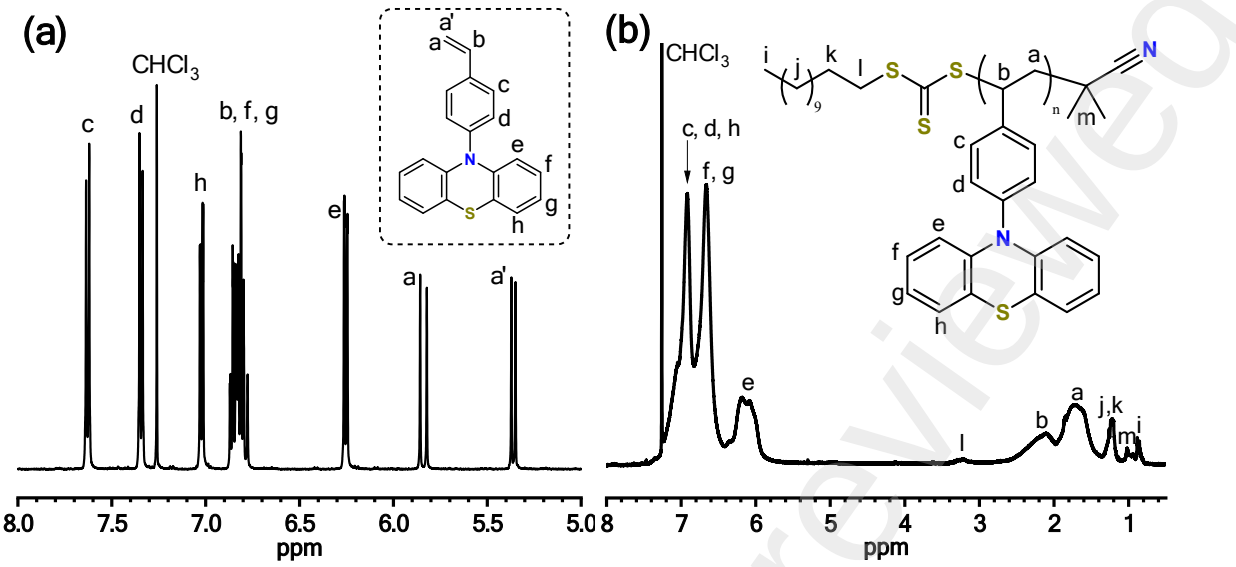

Figure 2. ^{1}H NMR spectra of (a) phenothiazine monomer (**M4**) and (b) corresponding polymer (**P4**, M_n = 5,200 g mol^{-1}; Đ = 1.22).

In the next stage of this study, RAFT polymerization of **M1**–**M4** monomers using the AIBN/DDMAT initiating system was investigated (Fig. 1b). DDMAT was selected as a chain-transfer agent due to the its high efficiency in controlled radical polymerization of a wide range of monomers including styrene and its derivatives [47,48].

In order to estimate the livingness of RAFT polymerization of **M1**–**M4**, it was investigated at different $[M]_0/[I]_0$ ratios (40, 100 and 500). The first-order kinetic plots describing these RAFT polymerizations are shown in Fig. 3, Fig. S2. The first-order plots are linear for all processes investigated, indicating that termination doesn't occur, and concentration of active species remains constant. As can be anticipated, the reaction rate decreases with an increase in $[M]_0/[I]_0$ ratio for each monomer studied that is associated with a decrease in concentration of initiator as compared to concentration of monomer (Fig. 3a, Fig. S2). Interestingly, the polymerization of **M1**, **M2**, **M4** proceed roughly with the same rate: the apparent rate constant ($k_{p.\,app}$) calculated from slope of first order plots (Fig. 3b) is about 20×10^2 h^{-1}. On the other hand, the polymerization of **M3** is almost two times faster than polymerization of **M1**, **M2**, **M4** (Fig. 3b).

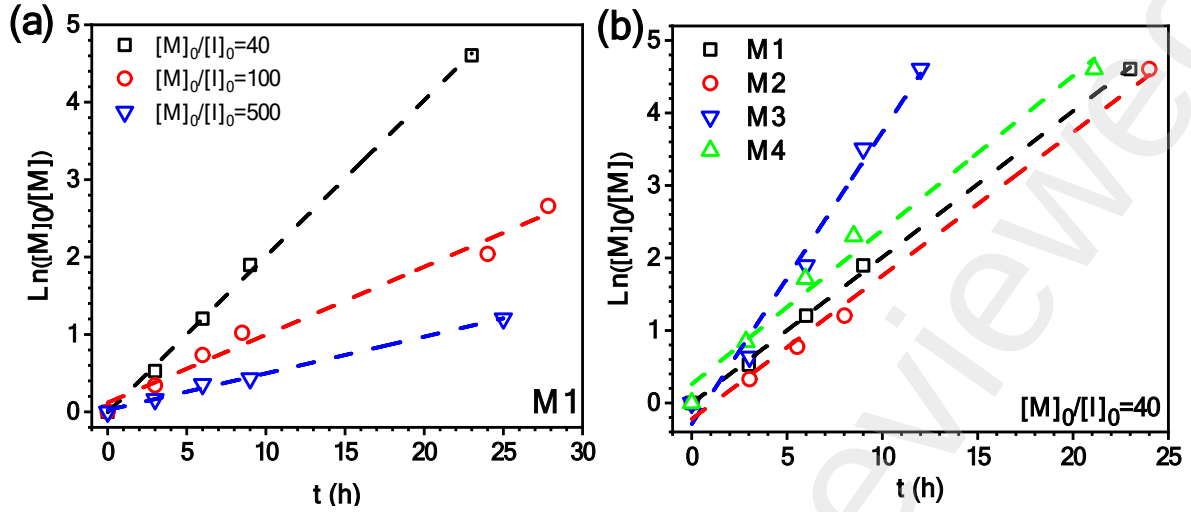

Figure 3. (**a**) First-order plots for polymerization of **M1** at $[M]_0/[I]_0$ = 40, 100 and 500 and (**b**) **M1**–**M4** at $[M]_0/[I]_0$ = 40 using the AIBN/DDMAT initiating system at 70 °C in cyclohexanone. Polymerization conditions: $[M]_0$ = 1 M, $[DDMAT]_0/[AIBN]_0$ = 3, $[I]_0 = [DDMAT]_0 + 2\cdot[AIBN]_0$.

In order to explain the observed kinetic patterns in the investigated polymerization processes, structures of corresponding propagating radicals (**R1** – **R4**) were optimized and their spin density distribution was modeled using 6-31G(d)/m06 method. The computed simulations are presented in Fig. 4. For all monomers the spin density is mostly distributed over styrene fragments (Fig. 4), but a small stabilization of radical by carbazole moiety was observed for **R1**, that is associated with d_a = 53° allowing π-systems of carbazole and styrene to interact with each other. Comparison of **R2**–**R4** activities showed the higher values of NBO and Mulliken charges on α carbon atom of styrene-type radical for **R3** (acridan-containing particle), that indicates its higher nucleophilicity (Table S1). It also should be noted that ^{1}H NMR chemical shifts of protons at β carbon atom for **M3** (**a**, **a'**, Fig. S1) are observed in weaker field then that of the other monomers (**M1**, **M2**, **M4**), from which it follows that the charge on β carbon atom for **M3** will be more positive. Both observations could explain the higher ability of **M3** enter the radical homopolymerization: more nucleophilic radical (**R3**) reacts more easily with more positively charged **β-C** of **M3** [50].

Polymerization of each monomer with $[M]_0/[I]_0$ ratios of 40 and 100 are characterized by the linear increase of M_n(SEC) with increasing monomer conversion and relatively low dispersity (Đ = 1.20-1.35 for $[M]_0/[I]_0$ = 40 and Đ = 1.25-1.60 for $[M]_0/[I]_0$ = 100) (Fig. 5a). This observation indicates that RAFT-mediated polymerization of **M1**–**M4** proceeds in a living fashion providing polymers with the controlled molecular weight ($M_n \leq$ 17,000 g·mol^{-1}). In addition, SEC curves of all synthesized polymers are symmetrical and completely shift to the high molecular weight region with increasing monomer conversion (Fig. 5b) that confirms living nature of the polymerization. In contrast, the processes at $[M]_0/[I]_0$ = 500 are characterized by non-linearity of M_n vs. conversion dependences and high dispersity ($M_n \leq$ 52,000 g·mol^{-1}, Đ = 1.4-3.0) indicating that side reactions operated at such conditions.

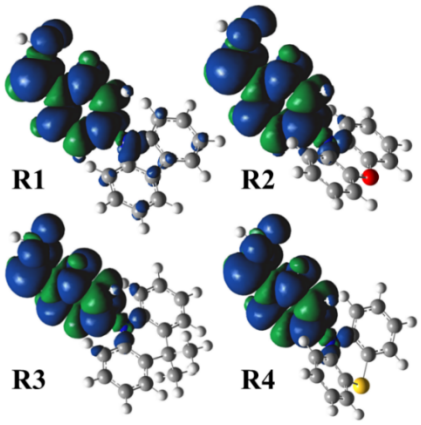

Figure 4. Spin density distribution on propagating macroradicals (**R1**–**R4**).

It should be also noted that experimental values of number-average molecular weight of all synthesized polymers were lower than theoretical ones (Fig. S3). The observed deviation is consistent with the known underestimation of M_n of the rigid polymers by SEC calibrated against polystyrene standards caused by the difference in hydrodynamic volumes between polystyrene and that of investigated polymers [51].

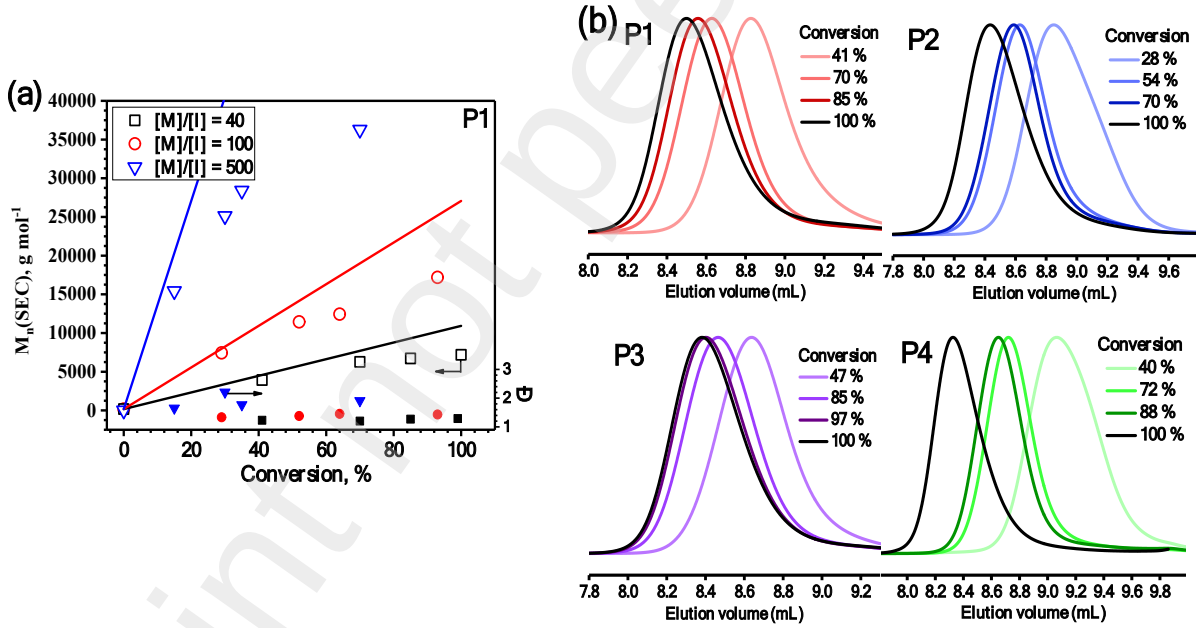

Figure 5. (**a**) M_n(SEC), Đ vs. conversion plots for polymerization of M1 using the AIBN/DDMAT initiating system at 70 °C in cyclohexanone at $[M]_0/[I]_0$ = 40, 100 and 500. Polymerization conditions: $[M]_0$ = 1 M, $[DDMAT]_0/[AIBN]_0$ = 3, $[I]_0 = [DDMAT]_0 + 2\cdot[AIBN]_0$. The straight lines correspond to the theoretical M_n. (**b**) SEC curves for **P1**–**P4** obtained at $[M]_0/[I]_0$ = 40.

The structures of the synthesized polymers (**P1**–**P4**) were investigated using ^{1}H NMR spectroscopy (Fig. 2b, Fig. S4). A notable aspect of the **P1**–**P4** spectra is the presence of signals indicative of the head (**m**, isobutyric or isobutironitrile) and the end (**i-l**, dodecyl trithiocarbonate) groups of the polymer main chain. Using more resolved signal of the end group (**l**), we were able to calculate the molecular weight of polymers by equation (1), while

the usage of other signals was complecated due to their mutual overlap (including the signal of CTA fragment in the head group).

$$M_n(NMR) = A\Omega + MM\frac{\int I(\mathbf{Ar})}{6\int I(\mathbf{l})} \quad (1)$$

where $A\Omega \cong 350$ is a sum of molecular weight of head and end groups; MM is a molecular weight of corresponding monomer; $\int I(\boldsymbol{Ar})$ or $I(\boldsymbol{l})$ – integral intensity of aromatic signals (**c**-**h**) or (**l**) signal under consideration. Obtained values are presented in Table S2. As it was anticipated, the M_n values calculated from ^{1}H NMR spectra are approximately twofold those calculated from SEC measurements. Nevertheless, these values are in good agreement with the theoretical molecular weights (M_n(theor.), Table S2).

3.2. Thermal properties

The thermal properties of the monomers (**M1** – **M4**) and the polymers (**P1** – **P4**) were studied by DSC and TGA (Fig. S5 – Fig.S7). The values of melting points (T_m), glass transition temperatures (T_g), and the temperatures at which 5% loss of mass was observed (T_{ID}) are summarized in Table 1. Monomers **M1**-**M4** showed endothermic melting signals in the first heating scans at 124, 162, 130 and 123 °C, respectively (Table 1, Fig S5). However, in the second heating scans only glass transitions were observed, indicating that during the first heating scan the monomers were subjected to the thermal self-polymerization (Fig. S5) [25,43]. This assumption was confirmed by analyzing the samples of the monomers after the first heating scans using size exclusion chromatography. According to the SEC data, thermal self-polymerization resulted in the formation of polymers with M_n(SEC) = 21,800 g·mol^{-1} (Đ = 5.4), M_n(SEC) = 20,700 g·mol^{-1} (Đ = 3.0), M_n(SEC) = 2,300 g·mol^{-1} (Đ = 17.5) and M_n(SEC) = 6,600 g·mol^{-1} (Đ = 25.5) from **M1**-**M4**, respectively (Table 1).

Table 1. Thermal characteristics of monomers and of the synthesized polymers.

Compound	MW[a], g·mol^{-1}	T_m[b] (°C)	T_g[c] (°C)	T_{ID}[d] (°C)
M1	269 / 21,800	124	180	393[e]
M2	285 / 20,700	162	154	413[e]
M3	311 / 2,300	130	158	394[e]
M4	301 / 6,600	123	154	393[e]
P1	7,200	–	200	404
P2	5,200	–	193	385
P3	7,700	–	202	381
P4	5,400	–	182	333

[a] Molecular weight for monomers and M_n(SEC) for polymers obtained using RAFT technique (**P1**-**P4**) or during DSC analysis via thermal self-polymerization of **M1**–**M4**; [b] determined by DSC from the first heating scan: scan rate 20 °C min^{-1}; [c] determined by DSC from second heating scan: scan rate 20 °C min^{-1}; [d] 5% weight loss determined by TGA: heating rate 20 °C min^{-1}. [e] 5% weight loss of polymer formed during the measurement.

Glass transition temperatures of **P1-P4** were observed to exceed T_m of the corresponding monomers **M1-M4** as well as T_g of the products of their thermal self-polymerization. The polymers were obtained as amorphous materials with high thermal stability (T_{ID} of up to 404 °C); no peaks due to crystallization and melting were observed in their DSC curves. It is noteworthy that for polymers **P2**–**P4**, T_{ID} was found to be somewhat lower than that observed for the products of the thermal self-polymerization of **M2-M4** (Table 1). This observation can be attributed to facilitating the polymer decomposition due to the presence of the labile RAFT end group at the temperatures above 300 °C [52].

3.3. DFT calculations and electrochemical properties

For a more thorough study of the electrochemical properties, quantum chemical calculations were performed. Molecular orbitals of the synthesized monomers (**M1**–**M4**), as well as monomer units in the main chain (**U1**–**U4**) of the obtained polymers were modeled using density functional theory (DFT) employing B3LYP/6-311++G(2df,2p)//B3LYP/6-31G(d,p) theory level. Computations revealed that monomers (**M1**–**M4**) LUMOs are localized mainly on the styrene part of the molecules. In the case of units **U1**–**U4** the vinyl group of styrene disappears, leading to a decrease in the conjugation system and, consequently, to an increase in energy of corresponding molecular orbital according to the particle in a box model [53, 54] (Table 2, Fig. 6a,S8). The effect is so significant that it leads to an exchange of LUMO and LUMO+1 positions in energy diagram, while the rest of the near-frontier orbitals remain unchanged (Table 2, Fig. 6a,S8). The principle of simulated evolution of frontier MO of monomers during polymerization is presented in Fig. 6a. As for HOMOs orbitals, in **M2**–**M4** and **U2**–**U4** they are located strictly on corresponding heterocyclic moieties, while in **M1** and **U1** HOMO covers the whole structure. This phenomenon could be explained by the same difference in the dihedral angle (d_a) between the heterocyclic and styrene (or benzene) fragments shortly described above: in **M2**–**M4** and **U2**–**U4** the planes of these fragments are perpendicular to each other turning the overlap integral to 0, while **M1** and **U1** are characterized by d_a = 55 and 57 degrees respectively, allowing an effective interaction between carbazole and styrene (or benzene) orbitals.

Table 2. Orbital properties of the synthesized monomers and polymers.

Compound	HOMO (calc.)[a], eV	I_p (CV)[b], eV	E_g[c], eV	E_A[d], eV	LUMO (calc.)[a], eV	LUMO+1 (calc.)[a], eV
M1	-5.67	-5.63	3.68	-1.95	-1.65	-1.19
M2	-5.00	-5.04	3.46	-1.58	-1.74	-1.02
M3	-5.21	-5.25	3.70	-1.55	-1.65	-0.93
M4	-5.26	-5.04	3.15	-1.89	-1.71	-1.05
P1	-5.61	-5.53	3.71	-1.82	-1.12	-0,86
P2	-4,94	-5.09	3.54	-1.55	-0.97	-0.82
P3	-5.14	-5.18	3.84	-1.34	-0.87	-0.72
P4	-5.19	-5.09	3.12	-1.97	-1.03	-0.73

[a] Computed by DFT using B3LYP/6-311++G(2df.2p)//B3LYP/6-31G(d.p) theory level (for polymers (**P1-P4**) simulation of the units structures (**U1-U4**) were used); [b] Ionization potentials obtained by CV data according

to the equation: $I_{P(CV)} = 4.8 + E^{ox}_{onset}$ vs Fc ; [c] measured as a cross-point of absorption and PL spectra in THF solutions; [d] Electron affinity obtained by CV data according to the equation: $E_A(CV) = I_P(CV) - E_g$

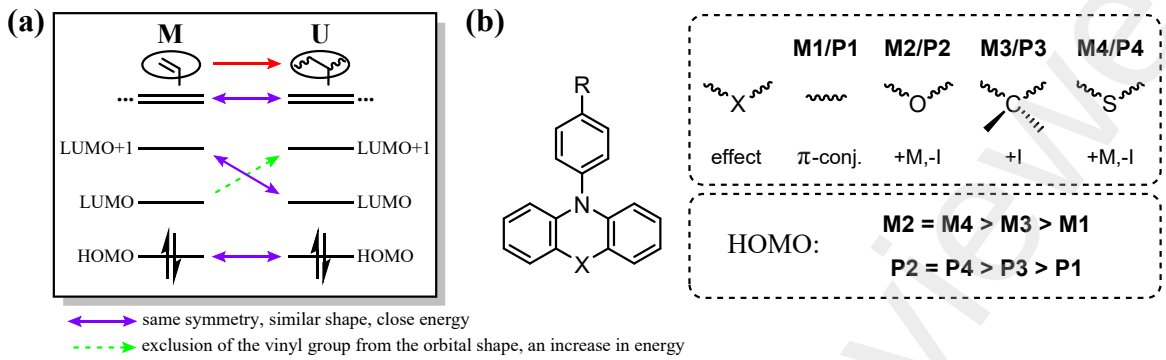

Figure 6. (**a**) Evolution of frontier MO of monomers during polymerization; (**b**) the influence of increment X in the dibenzoheterocyclic monomers and polymers on their HOMO energy.

The cyclic voltammetry (CV) measurements were performed for synthesized monomers (**M1**–**M4**) and corresponding polymers (**P1**–**P4**) in DCM at an inert atmosphere to determine the experimental ionization potential (I_p) values which are related to the HOMO energies. The half-wave potential of reversible oxidation waves of dilute solutions in dichloromethane of the studied materials with respect to ferrocene was used to obtain the I_p values (Fig. S9). The obtained values demonstrate the close agreement with computational ones (Table 2). The difference between experimental and calculated values does not exceed 0.2 eV which indicates the suitability of the applied theory level to predict orbital energies in such compounds. The influence of the increments X on HOMO energy of **M1**-**M4** and **P1**-**P4** is directly associated with its electronic effects (Fig. 6b, Table 2). The presence of a dimethylmethylene moiety displaying positive inductive effect (+I) (**M3** and **P3**) has been shown to result in an increase in the HOMO energy as compared to fully conjugated system (**M1**/**P1**). Furthermore, the incorporation of heteroatoms such as O or S (**M2**/**P2** or **M4**/**P4**, respectively), which exhibit competition between positive mesomeric (+M) and negative inductive (-I) effects, has been observed to result in an even greater increase in HOMO energy (Table 2). This is attributed to the superiority of the +M effect over the -I effect [25]. In summary, as it was demonstrated above, the HOMO energy of synthesized polymers can be easily tuned by the changing the substituent in the carbazole moiety.

The obtained CV data also allowed us to estimate the values of electron affinity energies (related to LUMO enrgies) of the studied compounds using the energy gap (E_g) values measured in the electronic spectra described below (Fig. 8, Fig. S10). However, the obtained values exhibited suboptimal convergence with the calculated values (Table 2). This is likely attributable to the contribution of non-HOMO-LUMO orbital transitions in the first electronic transition, resulting in a decrease of its energy.

For polymers and monomers containing carbazole, phenoxazine or phenothiazine fragments (**M1**, **M2**, **M4** and **P1**, **P2**, **P4**), CV peaks were characterized by a clear reversibility (Fig. S9). In the case of acridane-containing compounds (**M3** and **P3**), an

interesting phenomenon in their CV was discovered: during the first scan after one oxidative peak two reductive peaks were observed (Fig. 7a,b). However, the second oxidative peak appeared in further scans. It was characterized by lower applied potential and current values; in terms of shape, it appears to correspond the second reductive peak that has been identified in all scans. The aforementioned observations indicate that cation radicals formed by the oxidation of **M3** or **P3** are not stable and undergo chemical transformation. This effect has previously been observed for a number of 9,9-disubstituted acridane derivatives in a number of works [55,56]. In their study, the authors assumed that a condensation reaction may occur at the 2 and 7 positions of acridane moiety as the recombination of cation radicals followed by deprotonation. Therefore, we hypothesized that similar process could take place in case of **M3** and **P3** (Fig. 7c).

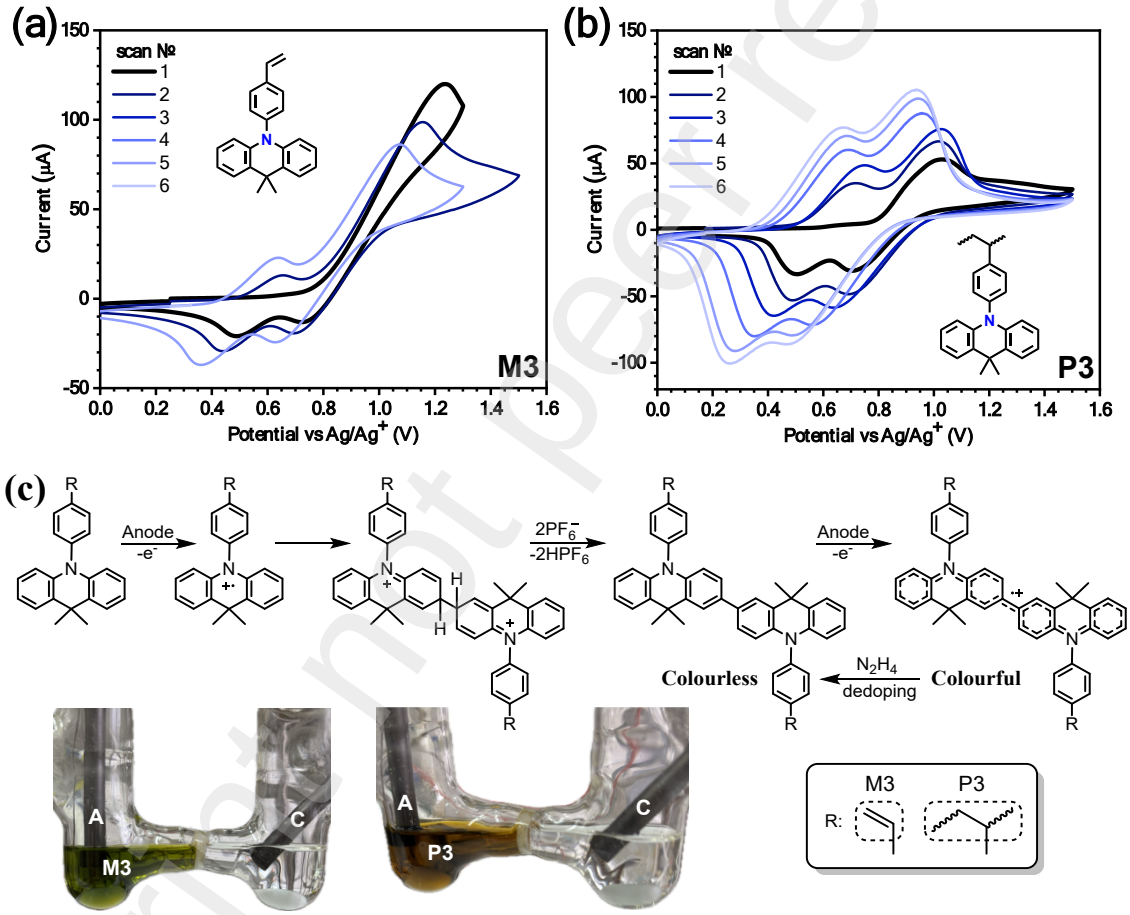

Figure 7. Cyclic voltammograms of (**a**) **M3** and (**b**) **P3** recorded at scan rate 50 mV s^{-1} vs. Ag/Ag^+ in a solution of Bu_4NPF_6 (0.1 M) in CH_2Cl_2; (**c**) scheme describing electrooxidative condensation of acridane moiety in **M3** and **P3**, and photos of corresponding elecrolyzates after 30 min of 1.0 V vs. Ag/Ag^+ potentiostatic regime.

In order to estimate the intensity of processes described above, we carried out the electrolysis of **M3** and **P3** solutions in DCM (with 0.1 M Bu_4NPF_6 as electrolyte). During the anodic oxidation in potentiostat regime at 1.0 V vs Ag/Ag^+ the solutions under examination began to exhibit a rapid change in coloration: from colorless to azure green for **M3** and to swamp green for **P3** (Fig. 7c). The addition of an excess of hydrazine hydrate

solution in methanol resulted in the complete discoloration of the system (dedoping), accompanied by precipitation of white polymer powder. This evidence suggests that the cation radicals are responsible for the color observed in the electrolyzate. It is noteworthy that the **P3** precipitate exhibited no further dissolution in any of the solvents, which can be attributed to the formation of a cross-linked architecture, which serves as an indirect confirmation of the proposed mechanism.

3.4. Photophysical properties of the solutions

The photophysical properties of the obtained polymers were then investigated. Absorption and photoluminescence spectra were recorded of the solutions in the solvents of varying polarities in order to evaluate solvatochromism. The results obtained were different from the anticipated ones (Table 3, Fig. 8). While the shapes of the PL bands differed, the maxima were found to be largely similar for most of the solutions of the same polymer. However, the polymer solutions in chloroform (and, in the case of **P3**, also in DCM) exhibited the anomalous red-shifted emission (Fig. 8, Fig. 9).

Table 3. Photophysical properties of the solutions of the polymers.

Polymer	λ_{max},[a] nm	Tol	$CHCl_3$	DCM	THF	Me_2CO	MeCN	PLQY,[c] %
P1	abs.	295, 325, 340	295, 330, 340	295, 325, 340	285, 320, 335	330, 345	296, 329, 343	-
	PL[b]	350, 360	350, 365, 450	350, 365	350, 365	350, 365	350, 365	26.99
P2	abs.	315	320, 400	325	280	335	325	-
	PL[b]	395	495	395, 485	375, 390	395	395	3.59
P3	abs.	290	290, 365	290	320	290	290	-
	PL[b]	375, 390	435	370, 445	395, 405	370, 385	370	8.05
P4	abs.	325	315	260, 315	310	330	260, 315	-
	PL[b]	450, 470	540, 560	450, 470	445, 470	445, 475	450, 480	0.49

[a] Wavelengths of absorption and PL maxima recorded in air at 298 K; [b] λ_{exc} = 300 nm; [c] measured by integrating sphere in THF solutions under air at 298 K.

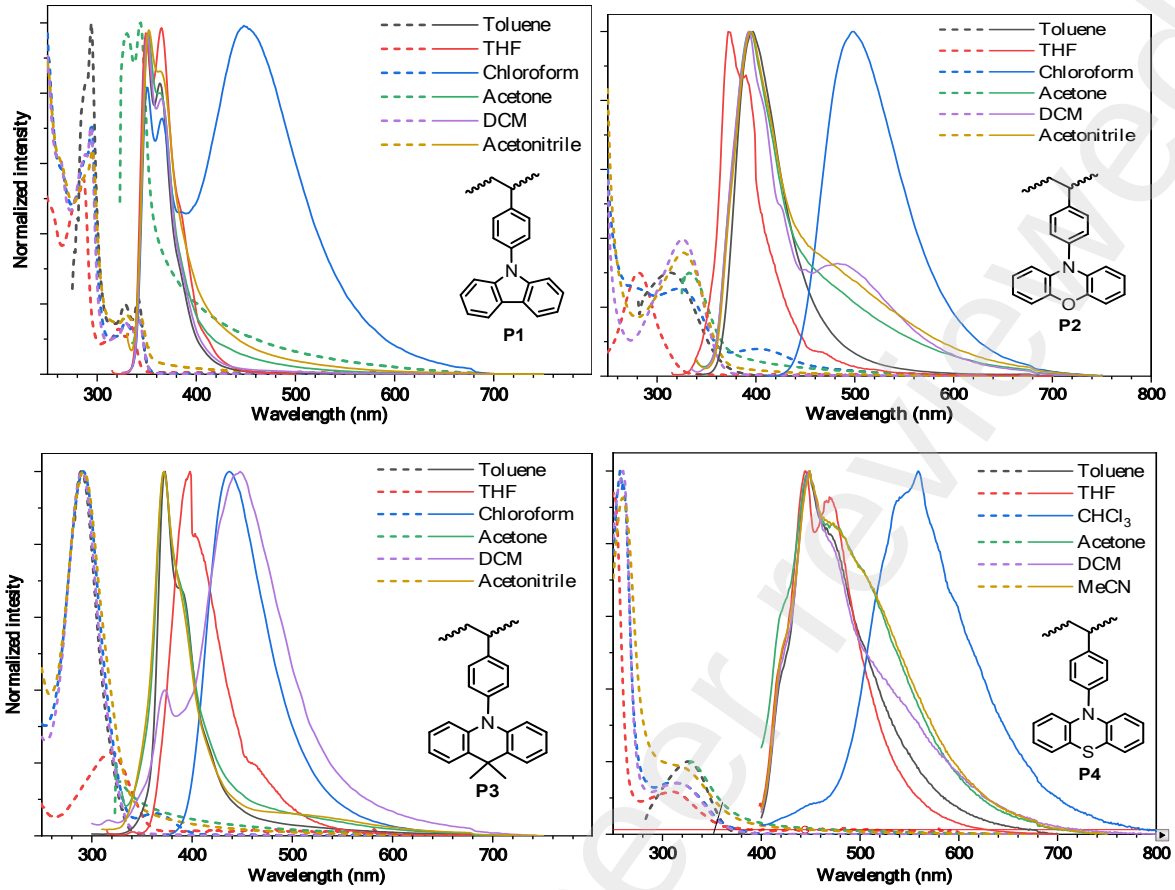

Figure 8. Combined UV−vis absorption (dash line) and photoluminescent (solid line, λ_{exc} = 300 nm) spectra of the solutions of **P1** – **P4** in the different solvents.

This observation can be explained by the potential interaction of excited polymer molecules with chloroform. It is established that a number of carbazole, phenoxazine, acridan and phenothiazine derivatives are capable of reducing halogen-containing compounds under the influence of electromagnetic radiation, thereby activating the C-Cl or C-Br bonds [8,10,55,57]. Consequently, they are employed as photocatalysts in photopolymerization (O-ATRP processes) and organic synthesis. [8,10,55]. Further corroboration of this hypothesis can be found in the study which demonstrated that excited carbazole molecules are susceptible to oxidation by tetrachloromethane [57]. It can be reasonably assumed that the longer wavelength emission is due to excimers formed between the excited polymer and chloroform (Fig. 9a).

In order to provide the quantitative substantiation of this assumption, it was necessary to measure the redox potential of the polymers under study in their excited triplet and singlet states. To achieve these objectives, fluorescence and phosphorescence spectra were recorded of THF solutions at 77 K. The obtained data are presented in Fig. 9c and Table 4. The energies of the singlet (S_1) and triplet (T_1) excited states, as well as the corresponding redox potentials ($E°(P^{+}/{}^{1}P^{*})$ and $E°(P^{+}/{}^{3}P^{*})$), were calculated on the basis of the obtained spectra.

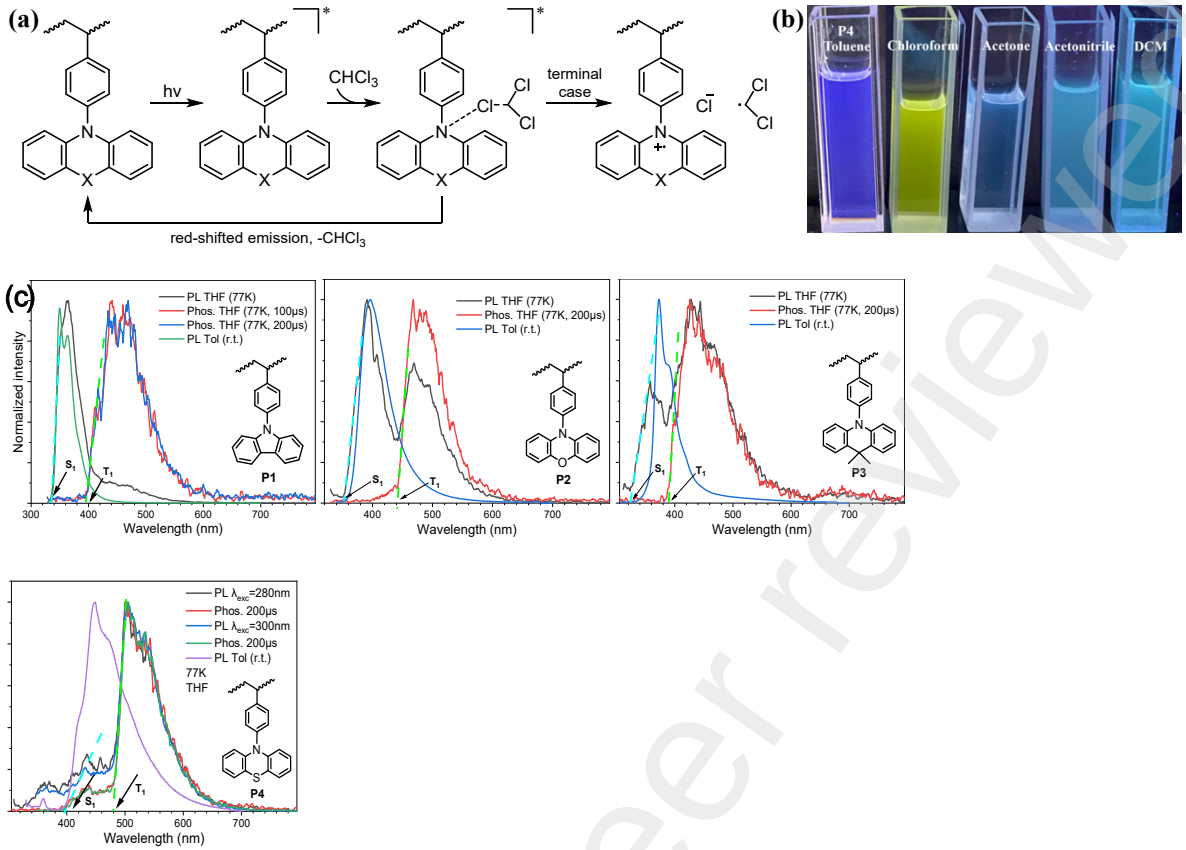

Figure 9. (**a**) Proposed mechanism of the formation of polymer-chloroform excimers; (**b**) photos of the solutions of **P4** in the different solvents under UV (λ_{max} = 350 nm) irradiation; (**c**) PL and phosphorescence spectra of THF solutions of **P1**-**P4** recorded at 77 K, λ_{exc} = 300 nm and 200 μs of delay, if the parameters are not specified.

Table 4. Electrochemical properties of the synthesized polymers.

Polymer	S_1[a], eV	T_1[a], eV	ΔE_{ST}, eV	$E°(P^+/P)$[b], V	$E°(P^+/{}^1P^*)$[b,c], V	$E°(P^+/{}^3P^*)$[b,c], V
P1	3.71	3.14	0.57	1.03	-2.68	-2,11
P2	3.54	2.81	0.73	0.60	-2.94	-2,21
P3	3.84	3.19	0.65	0.69	-3.15	-2,50
P4	3.12	2.58	0.54	0.60	-2.52	-1,98

[a] Measured from fluorescence and phosphorescence spectra; [b] vs. SCE; [c] calculated as $E°(P^+/P) - S_1$(or T_1)·ē.

The redox potentials of the excited singlet states of **P1**–**P4** are in the range of -3.15 to -2.52 V vs SCE (Table 4). Meanwhile, those of the triplet states are in the range of -2.50 to -1.98 V vs. SCE. Therefore, the reduction potential of both excited states is sufficient to reduce the carbon-chlorine bond in the chloroform molecule. According to the literature data its potential is of 0.3 V vs. SCE [58]. It is also worth of noting that among the polymers studied, the excited states of **P3** have the most expressed reducing properties, showing $E°(P^+/{}^1P^*)$ = -3.15 V and $E°(P^+/{}^3P^*)$ = -2.50 V vs. SCE. This observation may be the reason why this particular polymer is able to form excimers not only with the molecules of $CHCl_3$ but also with those of DCM, whose potential, according to the literature data, is of -1.5 V vs. SCE [59].

TD-DFT calculations were performed to identify relationship between the observed photophysical properties of **P1**–**P4** and their structures. In this way, natural transition orbitals (NTO) for the corresponding units (**U1**–**U4**) were visualized using B3LYP/6-311++G(2df.2p)//B3LYP/6-31G(d.p) theory level with PCM model for THF medium simulation. Computed NTO shapes are presented in Fig. 10. The examination of them reveals that the T_1 state of each polymer under investigation corresponds to the local excitation (LE) of π-electrons of the donor dibenzoheterocyclic groups. However, the S_0-S_1 transitions exhibited weak charge transfer (CT). In the case of **P1**, CT from the phenylene moiety to the carbazolyl group occured, while, in the cases of **P2**–**P4**, CT from the dibenzoheterocyclic groups to the phenylene fragment took place. The computational data allows to explain the observed near to the total absence of solvatochromic shifts of the spectra of the studied polymers thereby indicating LE-character of the excited states.

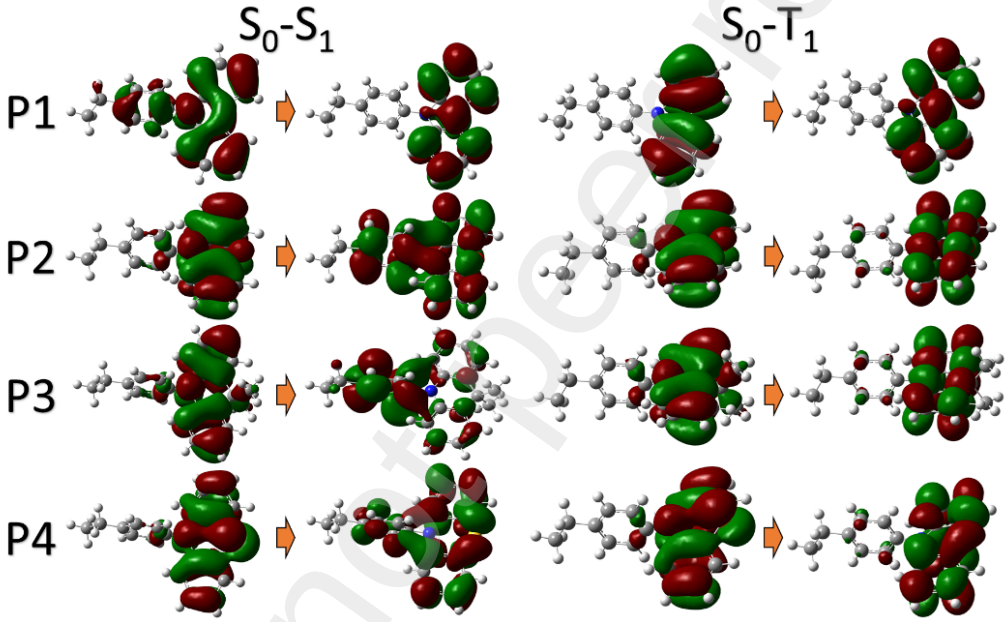

Figure 10. NTO shapes of S_1 and T_1 excited states of P1-P4.

Summarizing the obtained theoretical and experimental data, we can conclude that for the studied polymers the influence of the increments X (Fig. 6b) on the energies of the singlet and the triplet excited states shows the following tendency: **P3**>**P1**>**P**>**P4**. Therefore, most reliable method for the increase of the energy of excited states is the incorporation of a +I-donor moiety (such as disubstituted methylene) into the structure. Conversely, the incorporation of a heteroatom (O, S) results in ambiguous consequences being likely attributable to the different impact of the heteroatom +M-effect on the electron density of the ground state (S_0) and excited states (S_1 and T_1) with the more remote density [60].

Nevertheless, the reexamination of the acquired data reveals that the triplet energy and HOMO energy levels for the studied polymers exceed those of PVK (2.5 and -5.9 eV, respectively) [61], indicating that **P1**–**P4** are promising host materials for OLEDs fabrication [13,18,19]. Therefore, their properties in the solid state and their performance in various solution-processable devises were further investigated.

3.5. Electrooptical and photophysical properties of the films

The energy levels of the solid films of **P1**–**P4** were obtained by photoelectron emission (PE) spectroscopy in air. The ionisation potential (I_P^{PE}) of the solution-processed films **P1**–**P4** were taken from the corresponding PE spectra (Fig. 11a). The electron affinity (E_A^{PE}) values of the films were calculated using formula $E_A^{PE}=I_P^{PE}-E_g$. The I_P^{PE} and E_A^{PE} values of **P1**–**P4** are collected in Table 5. The films of **P1–P4** showed I_P^{PE} values in the range of 5.83-6.11 eV. These values are higher than I_P^{PE} values of many organic OLED emitters, including blue emitting ones [62]. The increase in I_P^{PE} during the transition from a single molecule to condensed state is the well-known phenomenon [63]. It is associated with the decrease in HOMO energy due to the polarization effect (van der Waals forces, π-π stacking, etc.) of the neighbouring molecules [64]. The quantitative characteristics of this effect (P_+) for the studied polymers are presented in Table 5. The P_+ values range from 0.58 to 0.82 eV, with the maximum value observed for **P4**. This phenomenon can be attributed to the presence of S atoms in its structure, which possess a higher polarizability and van der Waals radius compared to elements of the 2nd period [64].

The films of **P1**–**P4** showed E_A^{PE} values in the range of 2.3-2.64 eV, which are comparable with the values of I_P^{PE} of many organic OLED emitters [62, 65]. These results support the potential of **P1**–**P4** as the OLED hosts.

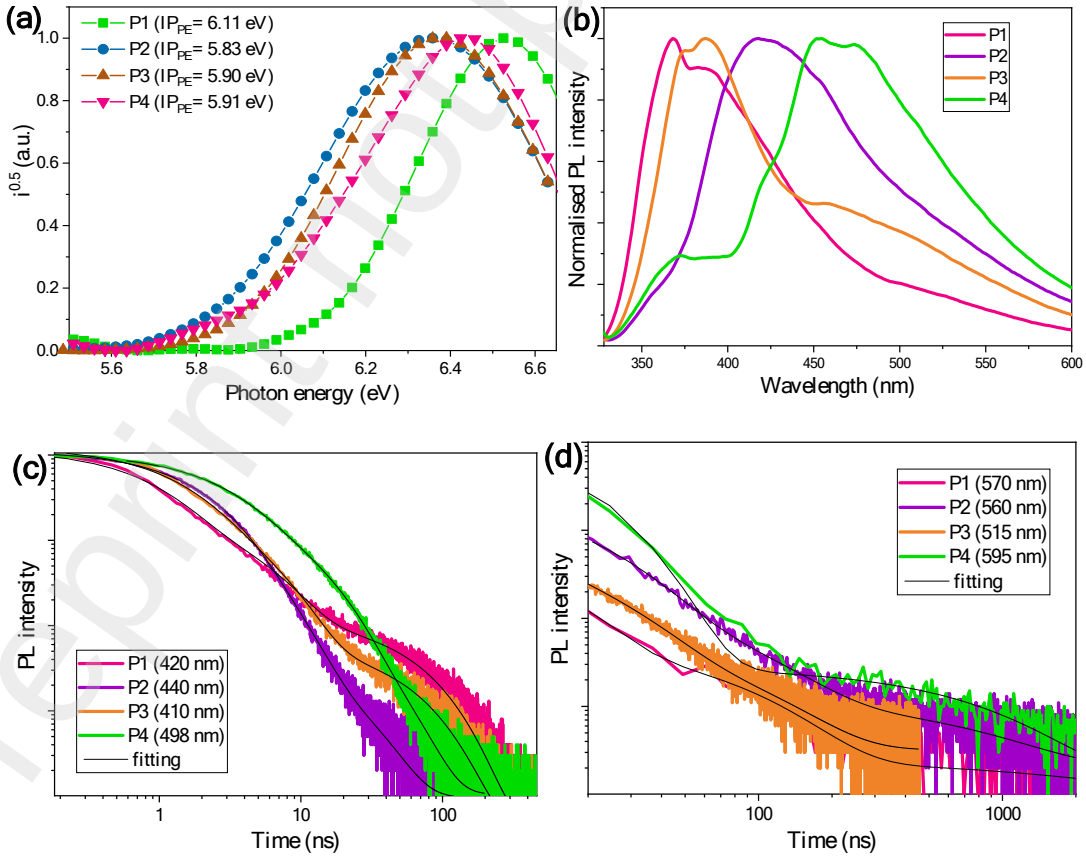

Figure 11. PE (**a**), PL spectra (**b**) and PL decay curves recorded at short (**c**) and long wavelengths of the spin-coated films of **P1–P4**.

PL spectra of neat films of **P1-P4** were characterised by high-energy and low-energy bands or shoulders (Fig. 11b). The high-energy emissions are similar to the emissions observed for the solutions of **P1**–**P4**. The low-energy emissions of the films can be attributed to excimer formation in the solid state [67]. PL decay curves of **P1**–**P4** were recorded at the shorter and the longer wavelengths (Fig. 11c,d). The long-lived emissions observed at the long wavelengths support the assumption of the excimer formation. The PL spectra, PL decay curves and fitting data of PL decay curves of the films of **P1**–**P4** recorded at the different conditions are collected in Fig. S11, Tables S3. For the estimation of the PL lifetimes of the films of **P1**–**P4**, the fittings for their PL decay curves were provided using the formula $y = A1\cdot\exp(-x/\tau_1) + A2\cdot\exp(-x/\tau_2) + A3\cdot\exp(-x/\tau_3)$, where x is τ, A1, A2 and A3 are the fractional intensities of prompt and delayed fluorescence; τ_1 is the lifetime of prompt fluorescence and τ_2 and τ_3 are lifetimes of delayed fluorescence. The equation (2) was used for the calculation of the average delayed fluorescence lifetimes [29]. The average lifetimes τ_{avg}^{film} are given in Table 5.

$$\tau = \frac{\sum A_i \tau_i^2}{\sum A_i \tau_i} \quad (2)$$

Table 5. Photophysical and electroluminescent parameters in the solid samples of **P1**–**P4** .

Compound	P1	P2	P3	P4
$\lambda_{abs\ (onset)}$, nm [a,b]	357	351	380	379
E_g, eV [b]	3.47	3.53	3.26	3.27
λ_{PL}^{film}, nm [a,c]	420	440	410	498
τ_{avg}^{film}, ns	17.30	2.63	8.12	6.63
χ^2	1.00	1.00	1.02	1.00
I_P^{PE}, eV [a]	6.11	5.83	5.90	5.91
P_+, eV	0.58	0.74	0.72	0.82
E_A^{PE}, eV	2.64	2.30	2.64	2.64
$\lambda_{EL}^{exciplex}$, nm [d]	538	568	530	593

[a] –Measured in air at 298 K; [b] measured from absorption spectra of the films; [c] λ_{ex} is 320 nm; [d] $\lambda_{EL}^{exciplex}$ is taken from EL spectra of devices II-P1-P4 (Figure 12c).

3.6. Charge-injecting, charge-transporting, exciplex-forming and electroluminescent properties.

For the estimation of charge-injecting, charge-transporting, exciplex-forming or electroluminescent (EL) properties of the polymers, we selected two types (I and II) of OLEDs with straightforward structures ITO/HAT-CN (8nm)/VM-35 (40nm)/EML (20nm) /TSPO1 (8nm)/TPBi (40nm)/LiF (1.7)/AL (devices I) and ITO/HAT-CN (8nm)/VM-35 (40nm)/EML (Polymers and POT2T (50%)) (20nm)/TSPO1 (8nm)/TPBi (40nm)/LiF

(1.7)/AL (devices II), respectively (Fig. 12a). Hole-transporting polymeric layer (VM-35) and light-emitting layer (EML) were spin-coated. The other functional layers were deposited in a vacuum. The materials used for the fabrication of OLEDs are described in the experiment section. Using the polymers **P1** – **P4** as hosts with high triplet energy levels of up to 3.19 eV (Table 4) for the previously developed TADF/TTA emitter 2,7-bis(9,9-dimethylacridin-10(9H)-yl)dibenzo[a,c]phenazine (AcDbp) [68], devices of the series I were fabricated. Their light-emitting layers consisted of AcDbp[20 wt.%] and **P1** (device **I-P1**), AcDbp[20 wt.%] and **P2** (device **I-P2**), AcDbp[20 wt.%] and **P3** (device **I-P3**), and of AcDbp[20 wt.%] and **P4** (device **I-P4**). Using the polymers as exciplex-forming materials (donors) in combination with the exciplex-forming acceptor 2,4,6-tris[3-(diphenylphosphinyl)phenyl]-1,3,5-triazine (PO-T2T) [69], devices of the series II were prepared. Their light-emitting layers consisted of **P1** and PO-T2T (device **II-P1**), **P2** and PO-T2T (device **II-P2**), **P3** and PO-T2T (device **II-P3**), **P4** and PO-T2T (device **II-P4**) (Fig. 12a). The donor-to-acceptor molar ratio was one to one. Devices **I-P1–P4** and **II-P1–P4** were characterized by very low brightnesses because of the lack of optimizations (Fig. 12b). This resulted in external quantum efficiencies below unity despite the fact that the used TADF emitters AcDbp and PO-T2T-based exciplexes showed EQE of over 20% in vacuum-deposited OLEDs [68,69]. This may be caused by the fact that AcDbp and PO-T2T were not ideally suited for the solution processable devices. Nevertheless, the charge-injecting and charge-transporting properties of polymers **P1–P4** can be relatively analyzed using the data collected for devices **I-P1–P4** and **II-P1–P4** (Fig. 12).

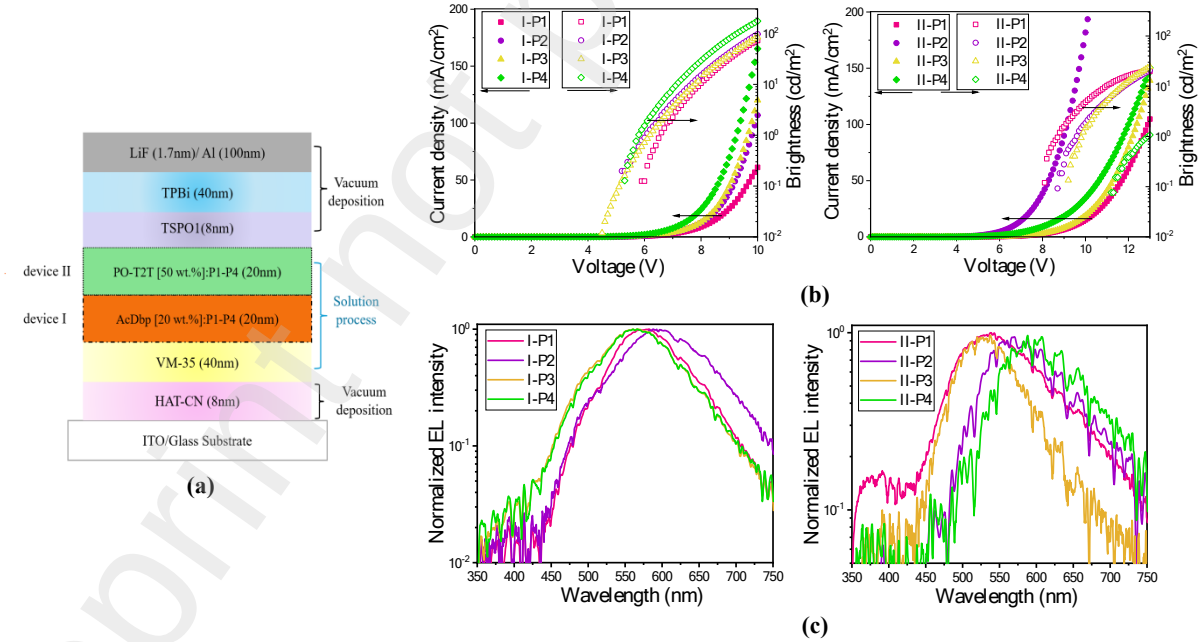

Figure 12. Schematical device structures (a), current density and brightness as the functions of voltage (b) and EL spectra of devices **I-P1–P4** and **II-P1–P4** (c).

The turn-on voltages of 6.58, 6.05, 6.17, and 5.8 V were observed for OLEDs **I-P1**, **I-P2, I-P3** and **I-P4**, respectively. The similar trend was observed for driving voltages of 8.1, 7.8, 7.8 and 7.2 V at the current density of 10 mA/cm^2 for devices **I-P1, I-P2**, **I-P3** and **I-P4**, respectively. This observation indicates that host **P4** had the best combination of charge-

injecting and charge-transporting properties. The charge-injecting and charge-transporting properties of **P2** are similar to those of **P3**. They are better than those of **P1**. The results obtained for **P1** are in agreement with the HOMO value of -5.53 eV estimated for this polymer. It is considerably lower than those estimated for the other polymers (Table 2).

The EL spectra of devices **I-P1–P4** are characterized by the emission of emitter AcDbp (Fig. 12c). The emission of hosts at ca. 350-450 nm was not observed even after EL spectra were rebuilt in log-log scales, indicating good energy transfer from host to guest. The EL spectra remain constant at the different voltages. It should be noted that the EL spectra of devices I peaked in the range of 565 to 596 nm despite the concentration of AcDbp (20 wt.%) was well controlled in solution-processable OLEDs. This means that the different polarity of **P1–P4** caused the differently situated peaks of EL spectra of devices **I-P1–P4**. **P2** caused the strongest shifts of charge-transfer emission of AcDbp when used in OLEDs as the host. Devices **II-P1–P4** allow the demonstration of exciplex forming properties of polymers **P1–P4**. The EL spectra of OLEDs peaked at the wavelengths of 525-598 nm (Table 5). The green-orange electroluminescence of devices **II-P1–P4** resulted from exciplexes formed between the polymers and PO-T2T. None of the functional materials of devices **II-P1–P4** are characterized by green-orange emission. The different colors of emissions of devices **II-P1–P4** can be explained by the different HOMO values of the studied polymers. The obtained information on EL and other properties of polymers **P1–P4** should be useful for the development of the next generation of polymeric hosts and polymeric exciplex-forming materials.

4. Conclusions

In this work, an approach for the synthesis of polymers with high triplet energy has been developed through the investigation of structure – properties relationship of the different dibenzoheterocyclic polymers. A series of styrene-type dibenzoheterocyclic monomers bearing carbazole, phenoxazine, 9,9-dimethylacridane and phenothiazine moieties were synthesized and subjected to the RAFT polymerization. It afforded well-defined polymers with $M_n(SEC) \leq 30{,}000$ g·mol^{-1}, moderate dispersity ($Đ = 1.2\text{-}1.6$), high glass transitions temperatures and high thermal stability ($T_g = 182\text{-}200$ °C and $T_{ID} = 333\text{-}404$ °C). It is demonstrated that incorporation into carbazole-like moieties of heteroatoms (O, S) possessing positive mesomeric effect is an efficient approach for the increase of the HOMO energy in dibenzoheterocyclic polymers. In contrast, the breaking of conjugation in carbazole moiety and the introduction of disubstituted methylene group possessing positive inductive effect allows to enhance the energies of excited states (both S_1 and T_1). The study of the photophysical properties of the solutions of the polymers reveals high values of HOMO (up to -5 eV), singlet (up to 3.8 eV) and triplet (up to 3.2 eV) energies. These characteristics endows the explored polymers with a unique property: the ability to form excimers with chloroform, which are characterized by an intense emission. The high reductive properties of the 9,9-dimethylacridane-based polymer (**P3**) excited states ($E°(P^+/{}^1P^*) = -3.15$ V vs. SCE,

$E°(P^+/^3P^*)$ = -2.50 V vs. SCE) enable its capacity to form excimers with dichloromethane. The high energetic values of **P3** are responsible for its ability to undergo step-growth coupling via electrooxidation at relatively low voltages (< 1 V vs. Ag/Ag^+). The distinctive properties of these polymers make them interesting to various fields including photocatalysis (especially, C-Hal photoactivation) and the synthesis of cross-linked electro- and photo-sensitive materials.

The triplet and HOMO energy levels of the studied polymers exceed those of commercially used PVK (T_1 = 2.5 eV, HOMO = -5.9 eV), indicating that the synthesized polymers are promising host materials for OLEDs (including blue ones) [13], despite of low quantum efficiency of devices fabricated in this work.

Acknowledgments: This work was supported by State Program for Scientific Research of Belarus "Chemical processes, reagents and technologies, bioregulators and bioorganic chemistry" (project 2.1.01.03) and State Committee on Science and Technology of the Republic of Belarus in framework of Belarus-India joint project X23INDG-013. This work has also received funding from the Research Council of Lithuania (LMTLT), agreement No S-MIP-22-78.

Conflicts of Interest: The authors declare no conflict of interest.

Supplementary Materials/ Appendix A

Supplementary data to this article can be found at [attached file] 3

References

[1] H. Jeong, H. Shin, J. Lee, B. Kim, Y.-I. Park, K.S. Yook, B.-K. An, J. Park, Recent progress in the use of fluorescent and phosphorescent organic compounds for organic light-emitting diode lighting, J. Photon. Energy 5 (2015) 057608. https://doi.org/10.1117/1.jpe.5.057608.

[2] S. Li, Y. Xie, Y. Yin, J. Chen, Y. Cao, S. Ying, Y. Liu, Z. Ren, S. Yan, Intramolecular Sensitization Assisting High-Efficiency TADF Conjugated Polymers with Accelerating Exciton Spin Flip for Solution-Processed Electroluminescent Devices, Macromolecules 57 (2024) 5253–5261. https://doi.org/10.1021/acs.macromol.4c00749.

[3] G. Hong, X. Gan, C. Leonhardt, Z. Zhang, J. Seibert, J.M. Busch, S. Bräse, A Brief History of OLEDs—Emitter Development and Industry Milestones, Adv. Mater. 33 (2021). https://doi.org/10.1002/adma.202005630.

[4] Z. Yang, Z. Mao, Z. Xie, Y. Zhang, S. Liu, J. Zhao, J. Xu, Z. Chi, M.P. Aldred, Recent advances in organic thermally activated delayed fluorescence materials, Chem. Soc. Rev. 46 (2017) 915–1016. https://doi.org/10.1039/c6cs00368k.

[5] S. Maiti, L.D.A. Siebbeles, Developments and Challenges Involving Triplet Transfer across Organic/Inorganic Heterojunctions for Singlet Fission and Photon Upconversion, J. Phys. Chem. Lett. 14 (2023) 11168–11176. https://doi.org/10.1021/acs.jpclett.3c03013.

[6] Y. Jin, Y. Zhang, Y. Liu, J. Xue, W. Li, J. Qiao, F. Zhang, Limitations and Perspectives on Triplet-Material-Based Organic Photovoltaic Devices, Adv. Mater. 31 (2019). https://doi.org/10.1002/adma.201900690.

[7] R.J. Hudson, A.N. Stuart, D.M. Huang, T.W. Kee, What Next for Singlet Fission in Photovoltaics? The Fate of Triplet and Triplet-Pair Excitons, J. Phys. Chem. C 126 (2022) 5369–5377. https://doi.org/10.1021/acs.jpcc.2c00273.

[8] D.A. Corbin, G.M. Miyake, Photoinduced Organocatalyzed Atom Transfer Radical Polymerization (O-ATRP): Precision Polymer Synthesis Using Organic Photoredox Catalysis, Chem. Rev. 122 (2021) 1830–1874. https://doi.org/10.1021/acs.chemrev.1c00603.

[9] S. Soly, B. Mistry, C. Murthy, Photo-mediated metal-free atom transfer radical polymerization: recent advances in organocatalysts and perfection towards polymer synthesis, Polym. Int. 71 (2021) 159–168. https://doi.org/10.1002/pi.6336.

[10] B.L. Buss, C. Lim, G.M. Miyake, Dimethyl Dihydroacridines as Photocatalysts in Organocatalyzed Atom Transfer Radical Polymerization of Acrylate Monomers, Angew. Chem. In.t Ed. 59 (2020) 3209–3217. https://doi.org/10.1002/anie.201910828.

[11] A. Bhattacherjee, M. Sneha, L. Lewis-Borrell, G. Amoruso, T.A.A. Oliver, J. Tyler, I.P. Clark, A.J. Orr-Ewing, Singlet and Triplet Contributions to the Excited-State Activities of Dihydrophenazine, Phenoxazine, and Phenothiazine Organocatalysts Used in Atom Transfer Radical Polymerization, J. Am. Chem. Soc. 143 (2021) 3613–3627. https://doi.org/10.1021/jacs.1c00279.

[12] Q. Wei, Z. Ge, B. Voit, Thermally Activated Delayed Fluorescent Polymers: Structures, Properties, and Applications in OLED Devices, Macromol. Rapid Commun. 40 (2018). https://doi.org/10.1002/marc.201800570.

[13] J. Ding, B. Zhang, J. Lü, Z. Xie, L. Wang, X. Jing, F. Wang, Solution-Processable Carbazole-Based Conjugated Dendritic Hosts for Power-Efficient Blue-Electrophosphorescent Devices, Adv. Mater. 21 (2009) 4983–4986. https://doi.org/10.1002/adma.200902328.

[14] V.K. Singh, C. Yu, S. Badgujar, Y. Kim, Y. Kwon, D. Kim, J. Lee, T. Akhter, G. Thangavel, L.S. Park, J. Lee, P.C. Nandajan, R. Wannemacher, B. Milián-Medina, L. Lüer, K.S. Kim, J. Gierschner, M.S. Kwon, Highly efficient organic photocatalysts discovered via a computer-aided-design strategy for visible-light-driven atom transfer radical polymerization, Nat. Catal. 1 (2018) 794–804. https://doi.org/10.1038/s41929-018-0156-8.

[15] Y. Lee, C. Boyer, M.S. Kwon, Photocontrolled RAFT polymerization: past, present, and future, Chem. Soc. Rev. 52 (2023) 3035–3097. https://doi.org/10.1039/d1cs00069a.

[16] F. Strieth-Kalthoff, F. Glorius, Triplet Energy Transfer Photocatalysis: Unlocking the Next Level, Chem 6 (2020) 1888–1903. https://doi.org/10.1016/j.chempr.2020.07.010.

[17] J. Zhao, W. Wu, J. Sun, S. Guo, Triplet photosensitizers: from molecular design to applications, Chem. Soc. Rev. 42 (2013) 5323. https://doi.org/10.1039/c3cs35531d.

[18] W. Jae Jang, J.-H. Jang, D. Bin Kim, J. Mo Kim, H. Kang, B.-G. Kang, Well-defined triphenylamine-containing polymers as hole-transporting layers in solution-processable organic light-emitting diodes via living anionic polymerization, Eur. Polym. J. 216 (2024) 113284. https://doi.org/10.1016/j.eurpolymj.2024.113284.

[19] Y.-C. Chen, G.-S. Huang, C.-C. Hsiao, S.-A. Chen, High Triplet Energy Polymer as Host for Electrophosphorescence with High Efficiency, J. Am. Chem. Soc. 128 (2006) 8549–8558. https://doi.org/10.1021/ja060936t.

[20] M.J. Bennison, A.R. Collins, B. Zhang, R.C. Evans, Organic Polymer Hosts for Triplet–Triplet Annihilation Upconversion Systems, Macromolecules 54 (2021) 5287–5303. https://doi.org/10.1021/acs.macromol.1c00133.

[21] Y. Xie, Z. Li, Thermally Activated Delayed Fluorescent Polymers, J. Polym. Sci. Part A: Polym. Chem. 55 (2017) 575–584. https://doi.org/10.1002/pola.28448.

[22] B. Zhang, Y. Cheng, Recent Advances in Conjugated TADF Polymer Featuring in Backbone-Donor/Pendant-Acceptor Structure: Material and Device Perspectives, The Chemical Record 19 (2018) 1624–1643. https://doi.org/10.1002/tcr.201800152.

[23] Z. Wang, R. Kunthom, S.V. Kostjuk, H. Liu, Near-infrared-emitting silsesquioxane-based porous polymer containing thiophene for highly efficient adsorption and detection of iodine vapor and solution phase, Eur. Polym. J. 192 (2023) 112072. https://doi.org/10.1016/j.eurpolymj.2023.112072.

[24] M. Sarkar, S. Sarkar, M. Saha, K. Luvani, A. Patra, Intriguing Facets of Solution Processable Cross-Linked Porous Organic Polymers, Acc. Mater. Res. 5 (2024) 1353–1365. https://doi.org/10.1021/accountsmr.4c00197.

[25] R.S. Bernard, V. Andruleviciene, G.K. Belousov, A.A. Vaitusionak, U. Tsiko, D. Volyniuk, S.V. Kostjuk, R.H. Kublickas, J.V. Grazulevicius, Methoxy-substituted carbazole-based polymers obtained by RAFT polymerization for solution-processable organic light-emitting devices, Eur. Polym. J. 174 (2022) 111323. https://doi.org/10.1016/j.eurpolymj.2022.111323.

[26] E. Stanislovaityte, J. Simokaitiene, S. Raisys, H. Al-Attar, J.V. Grazulevicius, A.P. Monkman, V. Jankus, Carbazole based polymers as hosts for blue iridium emitters: synthesis, photophysics and high efficiency PLEDs, J. Mater. Chem. C 1 (2013) 8209. https://doi.org/10.1039/c3tc31441c.

[27] T. Chatterjee, K. Wong, Perspective on Host Materials for Thermally Activated Delayed Fluorescence Organic Light Emitting Diodes, Adv. Optical Mater. 7 (2018). https://doi.org/10.1002/adom.201800565.

[28] Y. Suzuki, Q. Zhang, C. Adachi, A solution-processable host material of 1,3-bis{3-[3-(9-carbazolyl)phenyl]-9-carbazolyl}benzene and its application in organic light-emitting diodes employing thermally activated delayed fluorescence, J. Mater. Chem. C 3 (2015) 1700–1706. https://doi.org/10.1039/c4tc02211d.

[29] L. Izzo, P. Lisa, O. Sacco, S. Pragliola, Synthesis of Di-Block Copolymers Poly (Propylene oxide)-block-Poly (9-(2,3-epoxypropyl) Carbazole) via Sequential Addition of Monomers in One Pot, Polymers 13 (2021) 763. https://doi.org/10.3390/polym13050763.

[30] N.B. McKeown, S. Badriya, M. Helliwell, M. Shkunov, The synthesis of robust, polymeric hole-transport materials from oligoarylamine substituted styrenes, J. Mater. Chem. 17 (2007) 2088. https://doi.org/10.1039/b614235d.

[31] M. Kim, S. Yoon, S.H. Han, R. Ansari, J. Kieffer, J.Y. Lee, J. Kim, Molecular Design Approach Managing Molecular Orbital Superposition for High Efficiency without Color Shift in Thermally Activated Delayed Fluorescent Organic Light-Emitting Diodes, Chemistry A European J 25 (2019) 1829–1834. https://doi.org/10.1002/chem.201805616.

[32] R.M. Pearson, C.-H. Lim, B.G. McCarthy, C.B. Musgrave, G.M. Miyake, Organocatalyzed Atom Transfer Radical Polymerization Using N-Aryl Phenoxazines as Photoredox Catalysts, J. Am. Chem. Soc. 138 (2016) 11399–11407. https://doi.org/10.1021/jacs.6b08068.

[33] J. Lee, N. Aizawa, M. Numata, C. Adachi, T. Yasuda, Versatile Molecular Functionalization for Inhibiting Concentration Quenching of Thermally Activated Delayed Fluorescence, Adv. Mater. 29 (2016). https://doi.org/10.1002/adma.201604856.

[34] M. Hung, K. Tsai, S. Sharma, J. Wu, S. Chen, Acridan-Grafted Poly(biphenyl germanium) with High Triplet Energy, Low Polarizability, and an External Heavy-Atom Effect for Highly Efficient Sky-Blue TADF Electroluminescence, Angew. Chem. Int. Ed. 131 (2019) 11439–11445. https://doi.org/10.1002/ange.201904433.

[35] Y. Song, R. Yu, X. Meng, L. He, Donor-σ-acceptor molecules with alkyl σ-linkers of different lengths: Exploration on the exciplex emission and their use for efficient organic light-emitting diodes, Dyes and Pigments 208 (2023) 110876. https://doi.org/10.1016/j.dyepig.2022.110876.

[36] F. Chen, J. Hu, X. Wang, S. Shao, L. Wang, X. Jing, F. Wang, Synthesis and Electroluminescent Properties of Through-Space Charge Transfer Polymers Containing Acridan Donor and Triarylboron Acceptors, Front. Chem. 7 (2019). https://doi.org/10.3389/fchem.2019.00854.

[37] D. Zhang, C. Zhao, Y. Zhang, X. Song, P. Wei, M. Cai, L. Duan, Highly Efficient Full-Color Thermally Activated Delayed Fluorescent Organic Light-Emitting Diodes: Extremely Low Efficiency Roll-Off Utilizing a Host with Small Singlet–Triplet Splitting, ACS Appl. Mater. Interfaces 9 (2017) 4769–4777. https://doi.org/10.1021/acsami.6b15272.

[38] S.M. Cho, K.M. Youn, H.I. Yang, S.H. Lee, K.R. Naveen, D. Karthik, H. Jeong, J.H. Kwon, Anthracene-dibenzofuran based electron transport type hosts for long lifetime multiple resonance pure blue OLEDs, Organic Electronics 105 (2022) 106501. https://doi.org/10.1016/j.orgel.2022.106501.

[39] T. Ito, H. Sasabe, Y. Nagai, Y. Watanabe, N. Onuma, J. Kido, A Series of Dibenzofuran-Based n-Type Exciplex Host Partners Realizing High-Efficiency and Stable Deep-Red Phosphorescent OLEDs, Chemistry A European J 25 (2019) 7308–7314. https://doi.org/10.1002/chem.201805907.

[40] C.Y. Park, S.H. Park, N.Y. Kwon, J.Y. Park, M.J. Kang, H. Kwak, J.H. Son, H.Y. Woo, C.S. Hong, M.J. Cho, D.H. Choi, Polymer Hosts Containing Carbazole-Dibenzothiophene-Based Pendants for Application in High-Performance Solution-Processed TADF-OLEDs, ACS Appl. Mater. Interfaces 16 (2024) 45242–45251. https://doi.org/10.1021/acsami.4c06324.

[41] Z. Zhao, J. Wang, Y. Liu, J. Liu, Z. Ren, S. Yan, Synthesis and performance of non-conjugated main-chain thermally activated delayed fluorescence polymers with arylsilanes as host, Organic Electronics 77 (2020) 105539. https://doi.org/10.1016/j.orgel.2019.105539.

[42] P.R. Bommireddy, N. Mameda, C.S. Musalikunta, Y.-W. Lee, Y. Suh, M. Godumala, S.-H. Park, Recent breakthroughs in non-conjugated polymers for thermally activated delayed fluorescent OLEDs: emitters, hosts, and hole-transport materials, Mater. Chem. Front. (2025). https://doi.org/10.1039/d4qm00720d.

[43] A.A. Vaitusionak, I.V. Vasilenko, G. Sych, A.V. Kashina, J. Simokaitiene, J.V. Grazulevicius, S.V. Kostjuk, Atom-transfer radical homo- and copolymerization of carbazole-substituted styrene and perfluorostyrene, Eur. Polym. J. 134 (2020) 109843. https://doi.org/10.1016/j.eurpolymj.2020.109843.

[44] J. Poisson, C.M. Tonge, N.R. Paisley, E.R. Sauvé, H. McMillan, S.V. Halldorson, Z.M. Hudson, Exploring the Scope of Through-Space Charge-Transfer Thermally Activated Delayed Fluorescence in Acrylic Donor–Acceptor Copolymers, Macromolecules 54 (2021) 2466–2476. https://doi.org/10.1021/acs.macromol.0c02494.

[45] I.V. Vasilenko, A.A. Vaitusionak, J. Sutaite, A. Tomkeviciene, J. Ostrauskaite, J.V. Grazulevicius, S.V. Kostjuk, Simultaneous step-growth and chain-growth cationic polymerization of styrenic monomers bearing carbazolyl groups, Polymer 129 (2017) 83–91. https://doi.org/10.1016/j.polymer.2017.09.036.

[46] A.A. Vaitusionak, I.V. Vasilenko, E. Jatautiene, J. Simokaitiene, A. Tomkeviciene, J. Ostrauskaite, J.V. Grazulevicius, S.V. Kostjuk, Organocatalytic controlled anionic ring-opening polymerization of carbazole-containing thiiranes, Eur. Polym. J. 117 (2019) 179–187. https://doi.org/10.1016/j.eurpolymj.2019.05.009.

[47] S. Perrier, 50th Anniversary Perspective: RAFT Polymerization—A User Guide, Macromolecules 50 (2017) 7433–7447. https://doi.org/10.1021/acs.macromol.7b00767.

[48] M.A. Harvison, A.B. Lowe, Combining RAFT Radical Polymerization and Click/Highly Efficient Coupling Chemistries: A Powerful Strategy for the Preparation of Novel Materials, Macromol. Rapid Commun. 32 (2011) 779–800. https://doi.org/10.1002/marc.201100156.

[49] J.T. Lai, D. Filla, R. Shea, Functional Polymers from Novel Carboxyl-Terminated Trithiocarbonates as Highly Efficient RAFT Agents, Macromolecules 35 (2002) 6754–6756. https://doi.org/10.1021/ma020362m.

[50] Moad, G.; Solomon, D. *The Chemistry of Radical Polymerization*, 2nd ed.; ELSEVIER Ltd: The Boulevard, Langford Lane Kidlington, Oxford, UK, 2007; pp. 16–28.

[51] T. Saito, M.A. Lusenkova, S. Matsuyama, K. Shimada, M. Itakura, K. Kishine, K. Sato, S. Kinugasa, Reliability of molecular weight determination methods for oligomers investigated using certified polystyrene reference materials, Polymer 45 (2004) 8355–8365. https://doi.org/10.1016/j.polymer.2004.10.004.

[52] H. Willcock, R.K. O'Reilly, End group removal and modification of RAFT polymers, Polym. Chem. 1 (2010) 149–157. https://doi.org/10.1039/b9py00340a.

[53] R.H. Friend, R.W. Gymer, A.B. Holmes, J.H. Burroughes, R.N. Marks, C. Taliani, D.D.C. Bradley, D.A.D. Santos, J.L. Brédas, M. Lögdlund, W.R. Salaneck, Electroluminescence in conjugated polymers, Nature 397 (1999) 121–128. https://doi.org/10.1038/16393.

[54] G.K. Belousov, A.A. Vaitusionak, I.V. Vasilenko, M. Ghasemi, V. Andruleviciene, A. Ivanchanka, D. Volyniuk, H. Kim, J.V. Grazulevicius, S.V. Kostjuk, Through-Space Charge-Transfer Thermally Activated Delayed Fluorescence Alternating Donor–Acceptor Copolymers for Nondoped Solution-Processable OLEDs, Macromolecules 56 (2023) 2686–2699. https://doi.org/10.1021/acs.macromol.2c02582.

[55] Y. Liu, Q. Chen, Y. Tong, Y. Ma, 9,9-Dimethyl Dihydroacridine-Based Organic Photocatalyst for Atom Transfer Radical Polymerization from Modifying "Unstable" Electron Donor, Macromolecules 53 (2020) 7053–7062. https://doi.org/10.1021/acs.macromol.0c00377.

[56] T.L. Andrew, T.M. Swager, Detection of Explosives via Photolytic Cleavage of Nitroesters and Nitramines, J. Org. Chem. 76 (2011) 2976–2993. https://doi.org/10.1021/jo200280c.

[57] B. Zelent, G. Durocher, One-electron photooxidation of carbazole in the presence of carbon tetrachloride, J. Org. Chem. 46 (1981) 1496–1499. https://doi.org/10.1021/jo00320a055.

[58] Z. Sun, B. Li, X. Hu, M. Shi, Q. Hou, Y. Peng, Electrochemical dechlorination of chloroform in neutral aqueous solution on palladium/foam-nickel and palladium/polymeric pyrrole film/foam-nickel electrodes, J. Env. Sci. 20 (2008) 268–272. https://doi.org/10.1016/s1001-0742(08)60042-x.

[59] C. Schotten, T.P. Nicholls, R.A. Bourne, N. Kapur, B.N. Nguyen, C.E. Willans, Making electrochemistry easily accessible to the synthetic chemist, Green Chem. 22 (2020) 3358–3375. https://doi.org/10.1039/d0gc01247e.

[60] S. Ray, P. Mondal, Electronic Substitution Effect on the Ground and Excited State Properties of Indole Chromophore: A Computational Study, ChemPhysChem 24 (2022). https://doi.org/10.1002/cphc.202200541.

[61] K. Brunner, A. van Dijken, H. Börner, J.J.A.M. Bastiaansen, N.M.M. Kiggen, B.M.W. Langeveld, Carbazole Compounds as Host Materials for Triplet Emitters in Organic Light-Emitting Diodes: Tuning the HOMO Level without Influencing the Triplet Energy in Small Molecules, J. Am. Chem. Soc. 126 (2004) 6035–6042. https://doi.org/10.1021/ja049883a.

[62] K. Kumar, Charge Transporting and Thermally Activated Delayed Fluorescence Materials for OLED Applications, Phys. Chem. Chem. Phys. 26 (2024) 3711–3754. https://doi.org/10.1039/d3cp03214k.

[63] Y. Gao, Surface Analytical Studies of Interfaces in Organic Semiconductor Devices, Mater. Sci. Eng.: R: Reports, 68 (2010) 39–87. https://doi.org/10.1016/j.mser.2010.01.001

[64] Y. Xu, P. Xu, D. Hu, Y. Ma, Recent Progress in Hot Exciton Materials for Organic Light-Emitting Diodes, Chem. Soc. Rev. 50 (2021) 1030–1069. https://doi.org/10.1039/D0CS00391C

[65] B.J. Topham, M. Kumar, Z.G. Soos, Ionization potentials of crystalline organic thin films: Position dependence due to molecular shape and charge redistribution, Chem. Phys. Let. 493 (2010) 251–254. https://doi.org/10.1016/j.cplett.2010.05.007.

[66] Kaplan, I.G. *Intermolecular Interactions: Physical Picture, Computational Methods and Model Potentials*, 1st ed.; John Wiley & Sons, Ltd: New Era House, 8 Oldlands Way, West Sussex, UK, 2006; pp. 25–79. https://doi.org/10.1002/047086334x.ch2.

[67] R.M. Young, M.R. Wasielewski, Mixed Electronic States in Molecular Dimers: Connecting Singlet Fission, Excimer Formation, and Symmetry-Breaking Charge Transfer, Acc. Chem. Res. 53 (2020) 1957–1968. https://doi.org/10.1021/acs.accounts.0c00397.

[68] V. Andruleviciene, K. Leitonas, D. Volyniuk, G. Sini, J.V. Grazulevicius, V. Getautis, TADF versus TTA emission mechanisms in acridan and carbazole-substituted dibenzo[a,c]phenazines: Towards triplet harvesting emitters and hosts, Chemical Engineering Journal 417 (2021) 127902. https://doi.org/10.1016/j.cej.2020.127902.

[69] W.-Y. Hung, G.-C. Fang, S.-W. Lin, S.-H. Cheng, K.-T. Wong, T.-Y. Kuo, P.-T. Chou, The First Tandem, All-exciplex-based WOLED, Sci. Rep. 4 (2014). https://doi.org/10.1038/srep05161.